


Damage identification of cracked reinforced concrete beams through frequency shift

Andrea Benedetti  · Giacomo Pignagnoli · Mirco Tarozzi

Received: 18 June 2018 / Accepted: 15 October 2018 / Published online: 23 October 2018
© RILEM 2018

Abstract The safety evaluation of reinforced concrete (RC) bridges is of the outmost importance, both for the early warning of critical states below a given safety margin and owing to plan maintenance cycles of the infrastructural network. Structural health monitoring based on dynamic testing has become widespread in the last 20 years, leading to very effective operational algorithms able to extract valuable structural features from the recorded signals. However, although in principle it is possible to identify position and severity of the damage by using a finite element model, still some identification issues are unresolved due to the non-linear nature of the oscillations of a cracked beam. In fact, the available experimental data show, for a given damage pattern, a significant underestimation of the natural frequencies given by cracked beam numerical models. This paper presents an approximate solution for the problem of a vibrating damaged RC beam with opening–closing (breathing) cracks. The solution is based on the static equivalence of the kinetic energy and allows incorporating most of the features of a beam loaded above the cracking limit and oscillating under the self-weight with breathing cracks. The comparison with a wide data set collected

in the literature points out the predictive capability of the developed analytical formulas. An independent test confirms the theoretical results.

Keywords RC beam · Breathing crack · Dynamic test · Damage detection · Frequency shift

1 Introduction

The problem of ensuring bridge safety, either in terms of early warning of critical conditions or of maintenance scheduling, has a long history. A very simple and direct insight can be gained by accessing the page “List of bridge failures” on Wikipedia [1], where a large repository of news, photos and data is available.

Analysing the period 1950–2013, the average number of collapses with casualties and injured is two per year, with an average of 36 killed and 38 injured every year, and those numbers are steadily increasing, mainly as a consequence of the increase in number and age of bridges, but also due to the growth of vehicle weight and passages (Fig. 1). Moreover, no structural configuration is free from danger (Fig. 2).

The change in vibration frequency caused by damages in structural elements has always attracted the interest of researchers as a viable tool for the serviceability assessment of structural parts. For instance, this technique can be used for the detection

A. Benedetti (✉) · G. Pignagnoli · M. Tarozzi
Department of Civil, Chemical, Environmental and
Materials Engineering, University of Bologna, Viale
Risorgimento 2, 40136 Bologna, Italy
e-mail: andrea.benedetti@unibo.it
URL: <https://www.unibo.it/sitoweb/andrea.benedetti/en>

Fig. 1 Yearly values of collapsed bridges 1950–2013 (from Wikipedia.org)

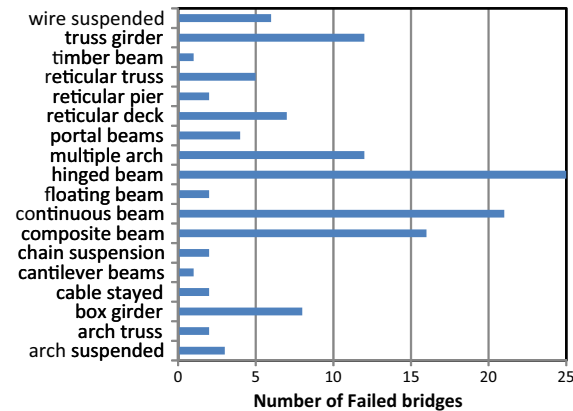
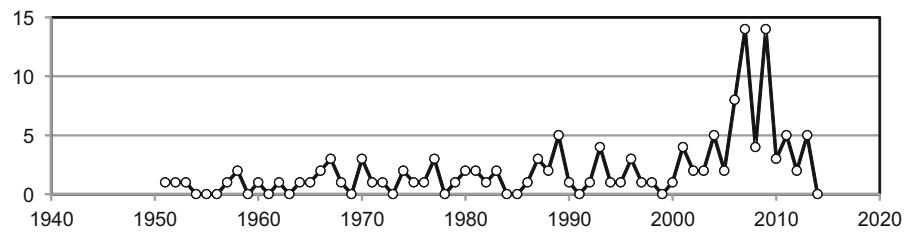


Fig. 2 Bridge failures 1950–2013 divided according to the structural form (from Wikipedia.org)

of localized cracks in metallic mechanical parts and the identification of damaged zones (in terms of position, extent, severity) in reinforced concrete bridges and buildings.

A very detailed state of the art report [2] lists more than 500 papers dealing with the first topic; for the case of bridge structures two literature reviews discuss most of the dynamic identification methods used even today [3, 4].

The recording of dynamic data on a structure subjected to environmental disturbances is a non-destructive testing method (NDT), since the response is linked to the stiffness distribution inside the structure. Thus, the health condition of a structure can be checked either by detecting changes in records kept at a given rate in time, or by extracting features of the stiffness distribution from the recorded signal.

Structural health monitoring (SHM) systems based on networks of few sensors (accelerometers, vibrometers, etc.) can collect big data sets in a relatively cheap way. Many other techniques exist for the local detection of the onset of cracks [5], but this information does not allow for a rating of the overall behavior.

However, concerning early detection of bridge damage states, there is a long list of problems to be addressed. Firstly, the structural weakening is a combination of many factors, such as cracking, load cycling and fatigue, environmental actions such as carbonation and freeze-thaw, support malfunctioning and foundation settlements. Secondly, temperature and humidity can influence the dynamic properties of the construction materials. Finally, the recorded signals are biased by unknown vehicle masses, by measurement errors, and by finite precision deconvolution techniques.

In the past, many experimental investigations pointed out that reinforced concrete structures in the non-linear range, starting with crack formation and ending at yielding of rebar, show a reduction of the natural frequencies from 0 to 25% of the uncracked values. This interval, however, is significantly less than expected, due to the presence of opening and closing cracks, the so called effect of “breathing cracks”.

Although the onset of cracking is characterized by a first significant frequency drop, temperature changes, chemical attacks and cyclic loading can modify the recorded values, hiding or emphasizing in some way the damage occurred in the structure.

In recent contributions, the problem of eliminating the temperature effect on the recorded signals has been solved effectively. On the one hand, the statistical analysis of the initial long term characterization of the bridge, can allow setting up a reference curve that expresses the natural frequencies as a function of temperature [6]. On the other hand, algorithms based on the co-integration concept are able to eliminate the temperature influence on the recorded signals [7]. This key ingredient allows for an effective monitoring, at least in order to plan bridge maintenance.

The deterioration occurring inside cracks mainly involves loss of tension stiffening of the concrete and aggregate interlock across crack faces. Therefore the

bond deterioration caused by cyclic loading or bar corrosion can increase the crack opening, thus reducing the crack closure stiffening effect [8]. Although these non-linear effects can be significant, the dynamic stiffening due to breathing still remains dominant when the crack opening is sufficiently small, as in the elastic range of the steel reinforcement with negligible rusting.

In this paper, the fundamental problem of expressing the stiffness deterioration in terms of frequency shift is reconsidered. The initial step is the study of a large set of experiments on simply supported ordinarily reinforced concrete beams discussed in the literature. The collected data encompass a wide range of material properties, beam geometries, loading patterns, and frequency extraction methods. In these investigations, the beam frequencies have been extracted at each loading step, up to the ultimate state of steel reinforcement yielding. By comparing the normalized non-dimensional load–frequency curves, a significant agreement can be observed among all the experiments. This is a key aspect allowing a robust comparison of the theoretical and numerical interpretations with the existing experimental data.

Then, in the framework of damage mechanics, the phenomenon of the “breathing cracks” is solved in an approximate but energetically consistent format. In this way, it is possible to build an analytical formula which expresses the frequency shift in terms of the maximum load experienced by the beam. It is to cite that simulations based on even complex models, able to predict the rigidity decay of cracked sections, fail in predicting the natural frequency of cracked beams, if they disregard the crack closure stiffening effect.

Finally it is to highlight that, since the proposed approach is based on the static equivalence of the kinetic energy, it can incorporate even progressive degradation effects such as chemical attacks or fatigue due to cyclic loading.

2 Analysis of the available experimental data

The selection of the comparison data set presents several problems due to the difficulties of retrieving missing values and as a consequence of the digitalization of data published in diagram form.

Table 1 presents the data extracted from references [8–17]. The meaning of the data is as follows:

- b, h, f_{ck} section base, height, and concrete compressive strength,
- A_s, f_{yk} steel reinforcement area and yielding strength,
- L, c beam length and distance between point loads,
- V_{exp}, f_{exp} beam ultimate shear and initial natural frequency,
- M_u, M_{cr} ultimate and cracking bending moments,
- $L_{D,max}$ length of the widest crack distribution.

In “Appendix”, all the non-dimensional load–frequency data are summarized in order to be used by other researchers in future works.

Askegaard and Langsoe [8] examined the frequency variation with respect to the load in beams deteriorated by freeze-thaw cycles. Van den Abeele and De Visscher [9] determined modal curvatures by using resonant acoustic spectroscopy. Maeck et al. [10] defined a parametric form of the length-wise variation of beam rigidity and evaluated the parameters by minimizing the error of the predicted modal frequencies through the inversion of the sensitivity matrix. Neild et al. [11] pointed out the strong frequency variation in correspondence of the cracking load. Tan [12] discussed the effect of “breathing cracks” in terms of bilinear and non-linear models. Koh et al. [13] used partitioned beam models for the interpretation of their observation, but it is fair to mention that their results do not match completely with the trend shown by all the other investigations. Massenzio et al. [14] examined the variation of five natural frequencies, but some inconsistencies are visible around the cracking point. Baghiee et al. [15] considered ordinary and FRP reinforced beams and used modal assurance criteria in order to detect the damage. Musial [16] presented results for beams with two reinforcement ratios but some inconsistency appears by comparing the two sets. Hamad et al. [17] presented very detailed experimental results, although the obtained frequencies are biased by the use of rubber supports for the beams. The interpretation is worked out by using fracture mechanics and partitioned beam elements. The model however does not incorporate breathing cracks, and therefore a specific adjusting coefficient is introduced owing to match the experimental results.

Figure 3 shows in graphical form the data contained in “Appendix”, in terms of the ratio of the damaged beam frequency to the initial one f_D/f_0 , and of



Table 1 Data of the collected experimental tests

References	Code	b (mm)	h (mm)	f_{ck} (MPa)	A_s (mm)	f_{yk} (MPa)	L (m)	c (m)	V_{exp} (kN)	f_{exp} (Hz)	M_{cr}/M_u (-)	$L_{D,max}$ (%)
Askegaard and Langsoe [8]	VBF	150	100	50	2 D10	500	3.00	1.00	6.0	22.5	0.258	83
Askegaard and Langsoe [8]	VXR	150	100	15	2 D10	500	3.00	1.00	5.0	19.1	0.130	91
Van den Abeele and De Visscher [9]	1	250	60	33	2 D10	500	0.99	0.15	5.7	161.0	0.187	84
Maeck et al. [10]	1	250	200	25	3 D16	500	3.60	0.00	50.7	22.3	0.193	81
Maeck et al. [10]	2	250	200	25	3 D16	500	5.70	2.00	25.3	21.9	0.193	87
Neild et al. [11]	A	200	105	38	3 D12	410	2.80	0.00	8.2	21.7	0.177	82
Neild et al. [11]	B	200	105	38	3 D12	410	2.80	0.00	8.2	22.4	0.177	82
Tan [12]	1	135	210	35	3 D10	500	2.80	1.00	21.5	92.0	0.282	82
Koh et al. [13]	1	500	150	44	6 D13	560	2.70	0.90	48.8	29.5	0.219	85
Massenzio et al. [14]	-	50	85	25	2 D4.5	500	0.67	0.23	5.0	530.0	0.195	87
Baghiee et al. [15]	B1–B3	150	200	20	2 D12	494	2.20	0.60	15.0	114.5	0.218	84
Baghiee et al. [15]	B4–B6	150	200	20	2 D16	483	2.20	0.60	30.0	108.8	0.177	87
Musial [16]	B-I	150	250	52	2 D12	563	3.00	0.00	14.0	91.0	0.378	62
Musial [16]	B-II	150	250	51	2 D12	563	3.00	0.00	14.0	90.0	0.376	62
Musial [16]	B-III	150	250	45	3 D10	548	3.00	0.00	14.0	91.0	0.349	65
Musial [16]	B-IV	150	250	41	3 D14	555	3.00	0.00	29.0	81.0	0.192	81
Hamad et al. [17]	BS-I	130	210	37	3 D10	541	2.70	0.70	20.9	43.0	0.223	83
Hamad et al. [17]	BS-II	130	210	37	3 D10	541	2.70	0.70	21.3	41.9	0.225	83
Hamad et al. [17]	BS-III	130	210	35	3 D10	541	2.70	0.70	20.3	42.6	0.216	84

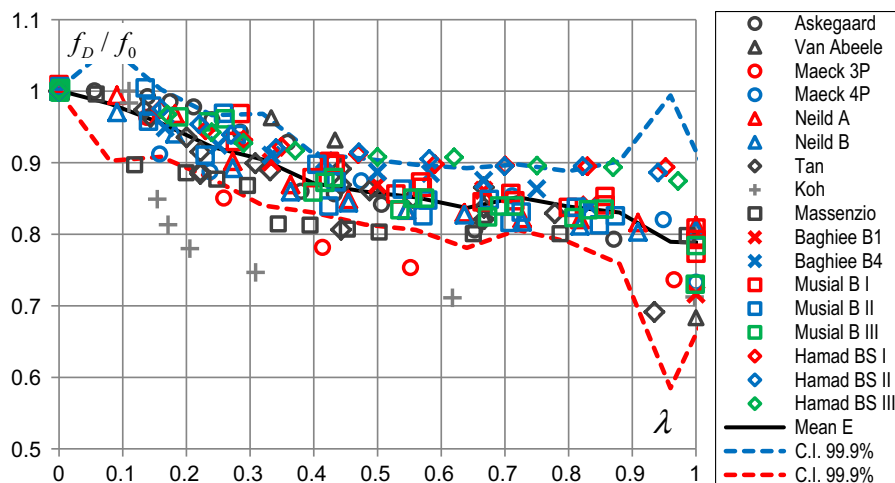


Fig. 3 Load—frequency plot of the selected experimental tests



the load amplification factor λ , where the ultimate load of the experiments is defined by $\lambda_u = 1.0$. The statistical analysis of the results indicates that almost all the data fall in a confidence interval of 99.9% of the mean, while the coefficient of variation COV is less than 5% over the whole range of data. Moreover, the data highlight a sharp increase in variance at the onset of cracking and near the failure.

As is apparent, Koh [13] data have a large deviation from the overall trend and exit from the confidence interval. Since the tested elements are very thin, this mismatch is probably due to the lack of crack closure effect.

In what follows, by using the principle of static equivalence of the kinetic energy, the mechanics of the damaged RC section will be used to set up the beam natural frequency. Some experiments of beams with a single crack will be reviewed with the aim of validating a model for the breathing crack phenomenon. The obtained interpretation will be used in building a formula able to characterize the relationship between load level increase and frequency decay.

3 Natural frequency of a damaged beam

The natural frequency of an Euler–Bernoulli beam with distributed or concentrated mass can be obtained through the equivalence of the kinetic energy of the vibration mode, and the potential energy of one equivalent deflected shape of the beam under a concentrated force [18].

If the mass of a simply supported beam is concentrated at the mid span, the equivalent force to be applied on the beam, leading to the equivalent vibration frequency, corresponds to 17/35 of the beam weight G .

Thus, the natural frequency of a simply supported beam can be expressed as a function of the maximum displacement occurring under this force. Considering a beam of length L , the displacement is:

$$\delta_0(L/2) = \frac{17G}{35} \cdot \frac{L^3}{48 \cdot EJ_0}, \quad (1)$$

where E and J_0 are respectively the elastic modulus and the inertia moment of the beam section in undamaged condition. The frequencies of the natural modes are finally obtained as:

$$f_n = \frac{n^2}{2\pi} \cdot \sqrt{\frac{g}{\delta_0}} \quad (2)$$

with g the gravity constant 9.81 m/s^2 , and n the number of half sinusoids contained in the beam length for a given mode.

If the beam presents a damaged part, the displacement is increased by the concentrated curvature spike resulting from the local loss of rigidity of the damaged length [10] and a decrease of the natural frequency is observed.

As an example, Fig. 4 shows the evolution of the experimental curvature obtained in [9] for a beam damaged with subsequent increasing load steps.

Figure 5 shows the reference geometry for the damaged beam, used in the following analytical elaboration. The beam displacement under the equivalent force is computed as the sum of the undamaged beam displacement δ_0 plus the incremental displacement δ_D caused by the localized curvature spike.

The damage engenders a total rotation $\Delta\chi \cdot L_D$ between the two rigid beam arms connecting the damaged zone to the supports. By enforcing the continuity equation of the rotation at the connecting sections, the displacement increase δ_D can be computed in a straightforward way. If the average tilt of the curved segment is indicated as ω , the compatibility equation is:

$$\left(\frac{\chi L_D}{2} + \omega\right) \cdot \left(a - \frac{L_D}{2}\right) = \left(\frac{\chi L_D}{2} - \omega\right) \cdot \left(b - \frac{L_D}{2}\right) - \omega \cdot L_D. \quad (3)$$

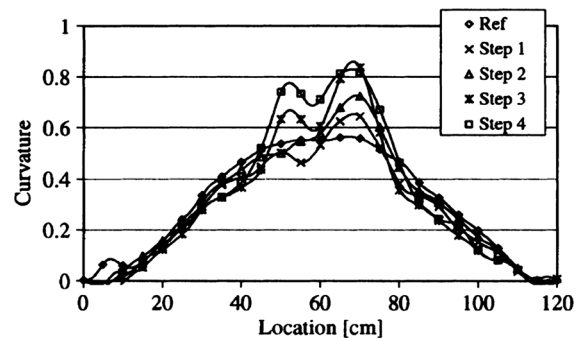


Fig. 4 Modal curvature spike obtained by the vibration mode of a damaged beam [9]

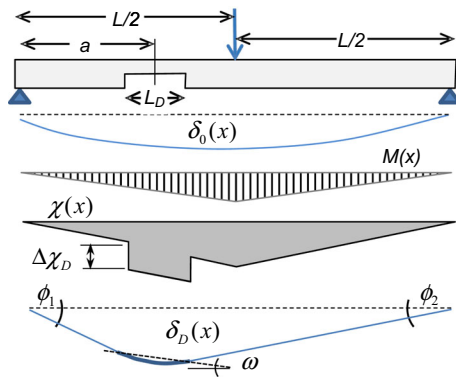


Fig. 5 Displacement components in a damaged beam

The solution is easily computed as:

$$\omega = \frac{1}{2} \Delta\chi_D L_D \frac{b-a}{L}, \tag{4}$$

and hence, the increase of displacement at the midpoint of the damaged zone, due to the curvature spike caused by the damage, holds:

$$\delta_D = \Delta\chi_D L_D \frac{L(2L - L_D)}{8L + 4L_D}. \tag{5}$$

By assuming that the bending moment is approximately constant on L_D , the curvature spike $\Delta\chi_D$ can be evaluated in terms of section rigidity variation:

$$\Delta\chi_D(a) = \frac{M(a)}{EJ_D} - \frac{M(a)}{EJ_0} = \chi(a) \cdot \left(\frac{EJ_0}{EJ_D} - 1 \right), \tag{6}$$

where EJ_0 is the section rigidity of the undamaged zones, while EJ_D is the one of the damaged part.

In conclusion the shifted frequency due to the localized damage can be evaluated from the total displacement $\delta_0 + \delta_D$ of Eqs. (1) and (5), in which the curvature spike is expressed as in Eq. (6); by factoring out the original first frequency, the damaged one holds:

$$f_{1,D} = f_1 \cdot \left[1 + 12 \frac{L_D}{L} \cdot \frac{2L - L_D}{8L + 4L_D} \cdot \left(\frac{EJ_0}{EJ_D} - 1 \right) \right]^{-1/2}. \tag{7}$$

A previous approximated version of this formula considered the rotation $\Delta\chi_D L_D$ concentrated in a hinge [19]. It has been extensively checked by the authors through numerical simulations, showing very good predictive behavior even in the case of circular arches [19].

3.1 Calculation of the damaged length

The evaluation of the damaged length requires the consideration of the bending moment distribution across the beam. Actually, when a beam is loaded in laboratory experiments, the positions of the forces are fixed, so that the bending moment varies in a proportional way among beam sections. However, in a real bridge beam, the diagram varies in a domain encompassing all cases from the dead weight distribution, to the load pattern of maximum intensity and extension in the serviceability conditions.

The damage in the beam cross sections occurs as an irreversible phenomenon once the cracking moment is exceeded under any of the possible loading patterns. If the maximum bending moment experienced by the beam is indicated as M_{max} and the cracking one as M_{cr} , the damaged length can be easily evaluated, if the shape of the diagram is known.

In the two relevant cases of uniformly distributed load and four point bending tests (4PBT) with a load spacing c , the damaged lengths are computed as:

$$L_D = L\sqrt{1 - \alpha} \text{ (uniform load)}, \tag{8.a}$$

$$L_D = c + (L - c)(1 - \alpha) \text{ (4PBT)}. \tag{8.b}$$

where α is the ratio M_{cr}/M_{max} . If we consider a reference load distribution, with an amplification factor λ holding 1.0 when the yielding condition of the beam mid span section is met, the link between α and λ is easily established:

$$\lambda = \frac{M_{max}}{M_y} = \frac{M_{max}}{M_{cr}} \cdot \frac{M_{cr}}{M_y} = \frac{\lambda_{cr}}{\alpha}. \tag{9}$$

The ratio λ_{cr} is expressing the fraction of the maximum load causing the first cracking of the beam.

In [11, 17] the distributions of the beam section rigidity at different load levels have been reconstructed on the basis of complete dynamic investigations. It is clearly shown that the damaged length is evolving up to 70–80% of the whole length approaching yielding of the reinforcement. When M_{max} attains the yielding value, α decreases to λ_{cr} with values in the range 0.20–0.30. As is indicated by Eq. (8.b), the damaged length increases to $L \cdot (1 - \alpha)$, i.e. more than 70% of the beam length.



3.2 Calculation of the damaged section rigidity

The calculation of the rigidity of the damaged sections requires the consideration of the loading path in the beam. Once the loading history pushes the bending moment distribution above the boundary of the local maxima experienced in the past, the size of the damaged region increases and the rigidity decreases. However, the load at which the beam frequency is measured, is normally near to the case of dead load only. Consequently, the damaged rigidity depends on the maximum moment occurred on the beam section, and this rigidity is larger than the tangent one given by the fully cracked section (see for instance [20]).

A detailed descriptions of the rigidity evolution can be found in [21, 22] as a function of the initial rigidity EJ_0 and the fully cracked section rigidity EJ_T . It is evident that bridges subjected to self-weight, with cracks formed by the previous loading history, will show beam stiffness values related with the section rigidity of the unloading branch (Fig. 6).

The secant rigidity is easily calculated from geometrical considerations:

$$EJ_D = \frac{M_{max}}{\frac{M_{cr}}{EJ_0} + \frac{M_{max}-M_{cr}}{EJ_T}} = \frac{EJ_T}{1 - \alpha \left(1 - \frac{EJ_T}{EJ_0}\right)}. \quad (10)$$

The smooth variation of the section rigidity after the first crack is pointed out in experiments described in [10, 20], where the evolution of the dynamic modulus is obtained from experimental data. This can be related to the progressive reduction of the concrete

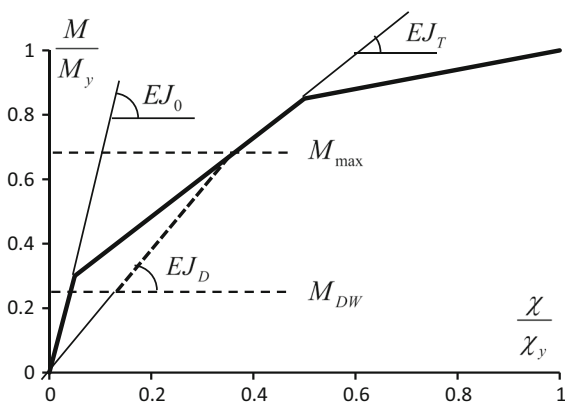


Fig. 6 Calculation of the damaged rigidity in the moment—curvature diagram

tension stiffening when the bending moment increases up to the yielding limit.

3.3 Frequency shift in a damaged beam

Consider a beam progressively damaged by increasing the load on it, but its natural frequency is measured in a reference situation with only the dead load present on the beam. Then the previous analyses can be linked together in order to derive a general formula for the natural frequency of a cracked beam, based on the load level experienced in the past by the beam. This is easily worked out by introducing in Eq. (7) L_D and EJ_D defined by Eqs. (8) and (10) in terms of α and λ .

As a particularization, a localized damaged zone is considered at the mid-span of the beam, caused by a concentrated load, such that $L_D = L \cdot (1 - \alpha)$. By introducing in Eq. (7) the cited expressions, the shifted frequency is obtained as a function of α :

$$f_{1,D} = f_1 \cdot \left[1 + 12 \frac{(1 - \alpha) \cdot (1 + \alpha)}{12 - 4\alpha} \cdot (1 - \alpha) \left(\frac{EJ_0}{EJ_T} - 1 \right) \right]^{-1/2}. \quad (11)$$

This damaged frequency is valid only when the cracks do not close during the vibration. This is the case for example of a running truck over a bridge such that the dynamic motion occurs without any upward displacement.

In most experimental tests in which the frequencies are recorded with the bare structure under the dead loads, the dynamic motion occurs with opening and closing of cracks, and therefore the non-linear effect of the crack face changing contact has to be considered.

4 The effect of breathing cracks

In literature, the phenomenon of crack opening and closure during the dynamic motion is named as “breathing crack”. The very first studies were motivated by some fatigue crashes of rotors used in the energy production plants [1]. Chondros [23] presented a detailed analysis of the simply supported beam with a crack, showing the difference of response when the crack is open or breathing.

An interesting comment of Tan [12] is based on Bendat’ well-known book [24]. It states that the interpretation of breathing cracks by using bilinear



crack constitutive laws, will not produce a non-linear behaviour. It can be concluded that the non-linear content of a breathing crack is concentrated only in the contact and release phases. This is evident from the steady vibration (Fig. 7) and phase diagrams (Fig. 8) reported from [25], in which the average harmonic behaviour is added.

In terms of the effect of a single crack, a suitable interpretation is possible based on the evaluation through the static equivalence. In a damaged vibrating element, the kinetic energy is constant during the oscillation inside the open or closed cracks phases, apart from the dissipation occurring during the locking—releasing phases. Then it exits an average frequency with which the energy is transferred between the two configurations.

A very simple interpretation is based on the assumption that the maximum displacement experienced by the beam during the oscillation is given by the cracked section rigidity when the motion releases the cracks, and by the original solid section rigidity, when the motion evolves with locked cracks.

Since these two deformed states are produced by the same energy, the breathing crack response is obtained by averaging the two displacements (b = breathing, o = open, c = closed):

$$f_b = \sqrt{\frac{2g}{\delta_c + \delta_o}} = \sqrt{\frac{2f_c^2 f_o^2}{f_c^2 + f_o^2}} \tag{12}$$

As a matter of example, some investigations reported by Chondros and Dimarogonas [23] are considered. In the following Table 2 the frequency ratios are listed for the three considered cases as a function of the non-dimensional crack size w/h ; the error resulting from Eq. (12) appears very small.

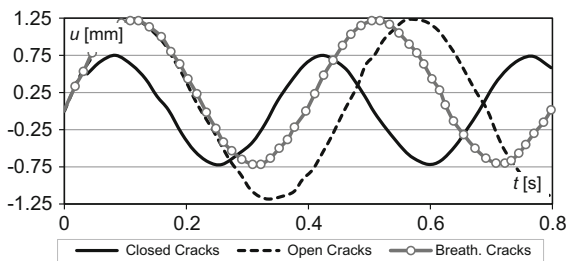


Fig. 7 The steady vibration of cracked sections (from [25]). The breathing crack response has a period near the average of the open and closed ones

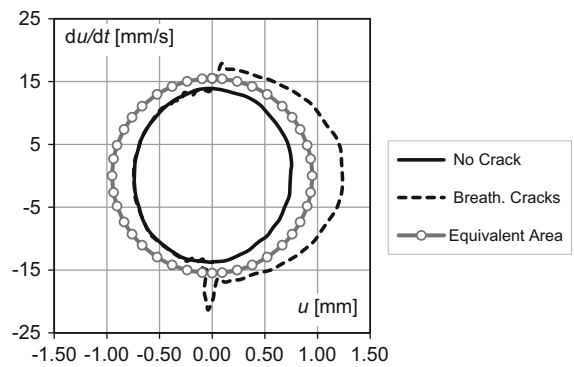


Fig. 8 The phase plot of the previous signals (from [25]). The average harmonic oscillation of an equivalent linear system is obtained by an equivalent area

The extension of the proposed formula to a beam with several cracks affecting the central part of the structure is based on a very simple deduction. Since Eq. (7) evaluates the increase of displacement for any extension of the damaged length, it holds even for the case of multiple adjacent cracks, and provides the vibrating frequency of a beam with several always open cracks of Eq. (11).

Therefore the averaging of the two displacements generated by the same kinetic energies is correctly carried out by Eq. (12), irrespective of the extension of the cracked length.

The static equivalent displacement is easily computed even by considering complex mechanical models of the cracked RC beam that take into account different degradation phenomena such as corrosion or cyclic loading (Table 3).

By example, the proposed combination formula (12) can easily deal with the stiffness degradation due to fatigue of the cracked beam caused by a large number of load repetitions. As a matter of fact, Kim [26] reported experimental values of frequency variation with the number of loading cycles, obtaining a significant decay:

It is easy to compare the frequency decay Δf of the measured frequency $f(n)$ at n cycles, with the reduction of the stiffness $k(n)$ extracted from the experimental displacements after n loading cycles. By computing the frequency variation as the square root of the stiffness variation, the comparison of Table 4 is obtained.

It is to cite that the effect of breathing cracks can be inferred even indirectly from literature results. For



Table 2 Comparison of experimental data from Chondros [23] and Eq. (12)

w/h	Closed crack	Open crack	Breathing crack	Theory	Error (%)
0.00	1	1.000	1.000	1.000	0.00
0.12	1	0.975	0.990	0.987	0.28
0.20	1	0.941	0.980	0.969	1.09
0.28	1	0.919	0.979	0.957	2.20
0.32	1	0.860	0.937	0.922	1.56
0.42	1	0.818	0.911	0.895	1.70
0.56	1	0.693	0.855	0.805	5.81

Table 3 Data of the fatigue frequency decay given by Kim [26]

Load cycles (<i>n</i>)	Frequency (Hz)	Decay (%)
0.00	45.35	0.00
0.20 × 10 ⁶	39.29	13.36
0.35 × 10 ⁶	35.28	22.21
2.00 × 10 ⁶	32.13	29.15

Table 4 Comparison of static and dynamic experimental data from [26]

<i>n</i> /10 ⁶	<i>k</i> (<i>n</i>)/ <i>k</i> (0)	<i>f</i> (<i>n</i>)/ <i>f</i> (0)	Δ <i>f</i> (%)	Exper.	Error (%)
0.00	1.000	1.000	0.0	–	
0.10	0.763	0.874	12.6	–	
0.20	0.691	0.831	16.9	13.4%	26.0
0.35	0.571	0.756	24.4	22.2%	10.1
0.60	0.459	0.678	32.2	–	
1.00	0.460	0.679	32.1	29.2%	10.3
2.00	0.460	0.681	31.9	29.2%	9.4

example consider the data of Xu and Castel [22]; they introduce a crack stiffening factor *D_{cc}* that is in the range {0, 1} with increasing values corresponding to an increase of beam deformability. The presented static loading cycles show the best fit with *D_{cc}* = 1 while the vibration frequencies are in agreement with *D_{cc}* = 0. The discrepancy can be easily explained by the stiffening effect of the breathing cracks, that let appear the beam deformability in dynamic motion lower than expected from static loading tests.

In what follows the formula (12) will be extensively used in the comparison of a wide the set of data previously discussed, with a very good general

agreement. Concerning the interpretation of the frequency evolution in RC beams with the cracking stages, very few numerical models that consider breathing cracks are present in the literature. The comparison of the proposed analytical interpretation is, in any case, in very good agreement even with existing numerical solutions. A precise evaluation of the breathing crack phenomenon in terms of FEM models will be presented in what follows.

5 Comparison of the theory with experimental literature results

The data presented in chapter 2 have been organized by performing the average of the results of each experimental investigation [8–17]. The experimental curves are compared with the solution of Eq. (11) (no crack closure), and with the solution with crack breathing included, as in Eq. (12). In particular, by merging the two formulas, the following opening—closing crack formula is obtained:

$$k_D = \frac{f_{1,D}}{f_1} = \sqrt{\frac{2}{2 + 12\eta \frac{(1-\alpha)^2 \cdot (1+\alpha)}{12-4\alpha}}} \tag{13}$$

where η is the factor $\left(\frac{EJ_0}{EJ_T} - 1\right)$, normally in the range {0.7, 1.5}, and α is obtained as λ_{cr}/λ by Eq. (9). Figure 9 shows the comparison.

The collected data can be approximated by using a logistic curve. By performing a best fit analysis, the following form is obtained:

$$k_D(\lambda) = \frac{f_D}{f_0} = 1.025 - \frac{0.25}{1 + 9 \cdot e^{-6.6\lambda}} \tag{14}$$

The error of the suggested interpolation form with respect to the whole data set is, on average, less than 0.33%.



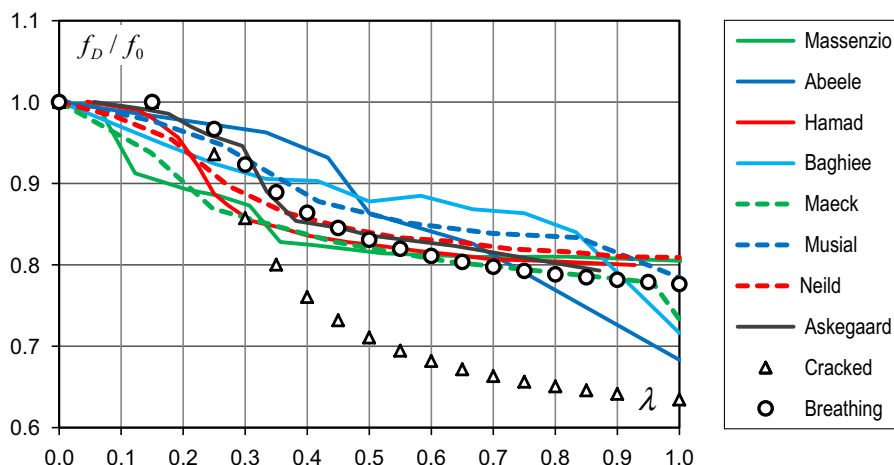


Fig. 9 Load—frequency plot of the proposed theory compared with the experimental tests

A numerical evaluation of the breathing crack phenomenon has been proposed by Gao et al. [27], by using an Expanded Distinct Element Method (EDEM). The software UDEC is used in forming a particle swarm mesh with connecting non-linear springs.

The best fit interpolation, the EDEM solution [27] and the analytical representation are compared in Fig. 10.

As is evident, the agreement among the three solutions is noticeable.

A simple approximated formula can be obtained by developing in series the function of α present in Eq. 13 around the value 1.0, i.e. when λ is near λ_{cr} :

$$\lambda = \frac{\lambda_{cr}}{1 - \sqrt{\frac{2}{3\eta} \cdot \frac{1 - k_D^2}{k_D^2}}} \tag{15}$$

By assuming by definition that λ holds 1.0 when the reinforcement is at the limit stress, this formula allows evaluating $k_{D,min}$, in terms of λ_{cr} and η only:

$$k_{D,min} = \frac{1}{\sqrt{1 + 1.5 \cdot \eta \cdot (1 - \lambda_{cr})^2}} \tag{16}$$

The formula (16) gives an approximated bound of the frequency shift that is to be expected when the beam enters in the collapse phase.

6 Verification by a new test

The previous theory has been verified with some experimental tests and numerical simulations completed by the authors. In particular some concrete beam with dimensions $150 \times 200 \times 2200 \text{ mm}^3$ were tested and simulated with different models in order to verify the proposed analytical results.

The laboratory tests concerned beams loaded in a 4PBT set up at different load levels up to yielding of the reinforcement. The loads corresponding to the cracking moment (M_{cr}) and the yielding moment (M_y), resulted in a maximum shear of 20 and 70 kN, respectively (Fig. 11).

Before and after the loading test, a set of signals given by ambient vibration were acquired and processed in order to extract the frequency content.

The vibration tests have been validated with three non-linear finite element models, namely: the solid

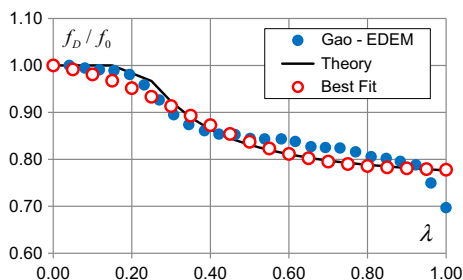


Fig. 10 Comparison of the proposed model with the best fit of data and a numerical model



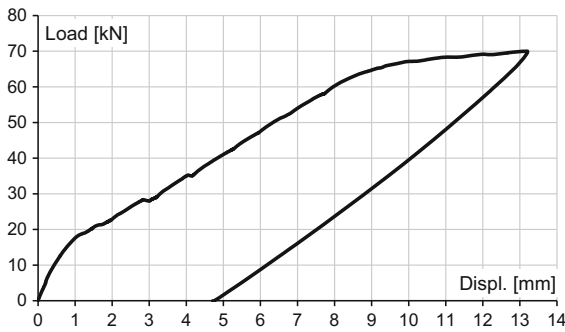


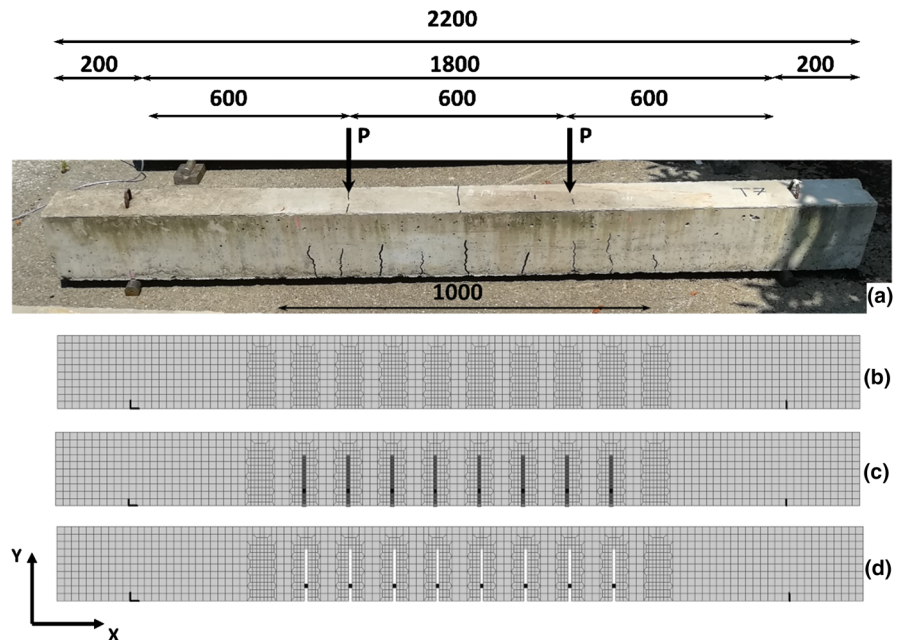
Fig. 11 Load cycle of the 4PBT performed on the experimental beam up to reinforcement yielding

beam, the beam with cracks steadily open and the one with breathing cracks.

The three FE models shown in the Fig. 12 have been created by considering the crack pattern of the real beam as a reference in order to place the cracks at a realistic distance along the beam. The behaviour of the breathing cracks has been modelled by using compression cut-off elements filling the slots simulating the cracks. The steel rebars have been included in the model by introducing truss elements at the distance from the beam bottom equal to the cover.

The bar debonding in the cracked zones has been simulated by considering a total length of 70 mm of the bars, bridging over the slots included in the

Fig. 12 Sketch of the loaded beam (a) and the three numerical models: solid beam (b), beam with compression only contact elements (c), beam with steadily open cracks (d)



numerical models. The data of the beam and the parameters that characterize the numerical models are listed in the Table 5.

In Fig. 13 are presented the FFT spectra of the non-linear calculations. Table 6 compares the experimental values with the numerical values and the predictions given by proposed formulas. A very good agreement can be observed among the three different analyses.

As is evident, the breathing crack hypothesis is supported not only by analytical theory, but also by the non-linear numerical models. Furthermore, the proposed model mock-up can be easily extended to more complex situations in order to study non-linear vibration problems.

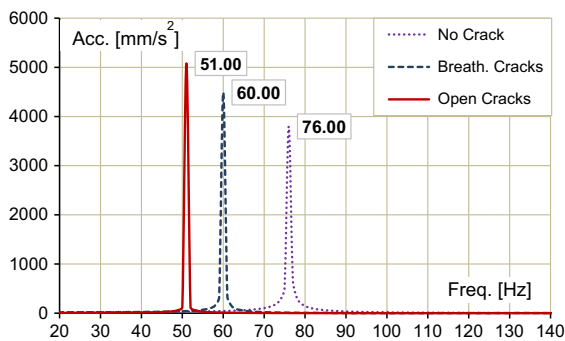
7 Conclusions

The evaluation of the main frequencies for simply supported RC beams with a cracked region is a challenging problem. In general, non-linear formulations based on the reduced rigidity of the cracked sections underestimate the frequency values due to the cyclic opening—locking of the cracks usually termed as “breathing cracks”. On the contrary, other factors such as freeze-thaw degradation or fatigue cycles can reduce consistently the natural frequency of cracked

Table 5 Materials of the beam and parameters assigned to the models

Material	Class	f_k (MPa)	E (MPa)	ρ (kg/m ³)	A_s (mm ²)	A_c (mm ²)
Concrete	C 20/25	20	20,000 ^a	2400	–	30,000
Steel	B450C	450	210,000	7850	226	–
Link	Compr. only	20	20,000	2400	–	1500

^aValue determined from ultrasonic tests

**Fig. 13** Comparison between the fundamental frequencies of the three numerical models

beams due to weakening of the concrete surrounding the tensile reinforcement.

The use of the static equivalence principle of the kinetic energy can help in building up a model in which all the influences are factored in the equivalent displacement evaluation, leading so to a general analytical formulation of the phenomenon. Since energy is a scalar quantity, a very simple hypothesis can be introduced for the evaluation of the alternate opening and locking of the cracks, based on the energy averaging of the two different phases. It is to cite that this hypothesis complies with the displacement averaging of the two configurations.

The formula of eq. (13), even if in an approximate form, is highly predictive of the observed behaviour as

in Fig. 9, and allows explaining the contribution of the crack cyclic closure on the final result.

A very large data base of experimental tests of simply supported damaged beams has been collected. Although the configurations show a wide range of the main parameters, the detected frequencies point out a well-defined trend as a function of the damage level. The comparison of the proposed formula with the statistical best fit of the population, and with a numerical solution based on the distinct element method, highlights the effectiveness of the adopted hypotheses.

The use of FEM models with non-linear elements reproducing the crack closure did allow explaining the observed experimental behaviour in quantitative terms.

In conclusion, the inversion of the series approximation of the analytical formula Eq. (13), allows evaluating the damage level of a bridge deck in terms of frequency shift with high reliability. The maximum frequency shift realistically shown by a bridge beam near the failure is predicted by Eq. (15).

The detection of dangerous conditions in real structures requires a good sensitivity of the monitored parameters. It is evident from the presented data that frequency drops can appear only at the onset of cracking or yielding. In this last condition however, the structure is too near to the collapse and therefore it is extremely risky to wait for this second borderline drop. The onset of a stable 10–15% frequency

Table 6 Comparison among the experimental frequencies and the numerical model results

Crack	Dyn. test	FE model	Err	Equations (2, 12)	Err (%)
Solid	75.60	76.00	0.53	79.00	4.49
Breathing	59.96	60.00	0.06	60.80	1.40
Open	51.21 ^a	51.00	0.41	51.90	1.34

^aValue obtained through the Eq. (12)



reduction (which probably is even steadily slightly increasing due to progressive bond deterioration), is the key response to look for. At this event, an immediate inspection and maintenance activity must be planned and carried out.

Acknowledgements This research has received the financial support from the ERA-NET Infravation 2014 research program through the SHAPE project (Predicting Strength Changes in Bridges from Frequency Data—Safety, Hazard, and Polyharmonic Evaluation) under Grant 31109806.004. The support of the Infravation program is gratefully acknowledged.

Compliance with ethical standards

Conflict of interest The authors declare that they have no conflict of interest.

Ethical standards The Project SHAPE and the research program Infravation completely comply with the ethical standards required by the European Community for research granting. This study does not contain any research done with humans or animals.

Informed consent Informed consent was obtained from all participants included in the study.

Appendix

Tables 7, 8, and 9 contain the non dimensional data of the points and curves shown in Figs. 3 and 9.

Table 7 Non dimensional load–frequency curves of the references [8, 12, 14]

Askegaard and Langsoe [8]						Massenzio et al. [14]						Tan [12]	
VBF-1		VBF-3		VXR-1		F_1		F_2		F_3		1	
λ	k_D	λ	k_D	λ	k_D	λ	k_D	λ	k_D	λ	k_D	λ	k_D
0.0565	1.0000	0.0568	1.0003	0.0557	1.0005	0.0000	1.0000	0.0000	1.0000	0.0000	0.9988	0.0000	1.0000
0.1230	0.9841	0.1395	0.9987	0.1390	0.9923	0.0606	0.9943	0.0585	0.9960	0.0691	0.9945	0.1338	0.9739
0.1725	0.9748	0.1819	0.9969	0.1743	0.9850	0.1191	0.8881	0.1188	0.8971	0.1296	0.9522	0.1438	0.9638
0.2161	0.9375	0.2115	0.9935	0.2114	0.9780	0.2005	0.8468	0.1997	0.8859	0.2188	0.9449	0.2003	0.9355
0.2322	0.9357	0.2457	0.9853	0.2400	0.9600	0.2524	0.8387	0.2478	0.8770	0.2734	0.9388	0.2220	0.8955
0.2931	0.9318	0.3089	0.9636	0.2847	0.9426	0.2974	0.8211	0.2960	0.8682	0.3280	0.9290	0.3083	0.8992
0.3138	0.8341	0.3312	0.9080	0.3590	0.9284	0.3476	0.7938	0.3442	0.8143	0.3777	0.8762	0.3315	0.8892
0.3734	0.8159	0.3924	0.8860	0.3800	0.8600	0.3978	0.7881	0.3941	0.8127	0.4414	0.8713	0.4429	0.8556
0.4955	0.8072	0.4376	0.8711	0.4323	0.8564	0.4567	0.7833	0.4527	0.8071	0.5051	0.8658	0.4877	0.8611
0.5000	0.8060	0.5000	0.8600	0.5063	0.8418	0.5070	0.7784	0.5026	0.8031	0.5560	0.8610	0.5558	0.8511
0.6144	0.8068	0.6442	0.8574	0.6526	0.8058	0.6560	0.7767	0.6506	0.8006	0.7234	0.8520	0.6671	0.8411
				0.8710	0.7929	0.7946	0.7742	0.7866	0.8006	0.8743	0.8552	0.7784	0.8292
						0.9905	0.7676	0.9862	0.7982	1.0425	0.8487	0.9347	0.6914



Table 8 Non dimensional load–frequency curves of the references [11, 15, 17]

Neild et al. [11]				Hamad et al. [17]						Baghiee et al. [15]			
A		B		BS-I		BS-II		BS-III		B1-12D-0L		B4-16D-0L	
λ	k_D	λ	k_D	λ	k_D	λ	k_D	λ	k_D	λ	k_D	λ	k_D
0.0000	1.0000	0.0000	1.0000	0.0000	1.0000	0.0000	0.9994	0.0000	1.0006	0.0000	1.0011	0.0000	1.0000
0.0909	0.9942	0.0909	0.9703	0.1594	0.9749	0.1605	0.9754	0.1703	0.9674	0.3333	0.9008	0.1667	0.9488
0.1818	0.9677	0.1818	0.9402	0.2299	0.9451	0.2202	0.9537	0.2397	0.9424	0.5000	0.8688	0.2500	0.9243
0.2727	0.9019	0.2727	0.8920	0.2896	0.9317	0.2701	0.9391	0.2896	0.9273	0.6667	0.8613	0.3333	0.9104
0.3636	0.8695	0.3636	0.8595	0.3492	0.9224	0.3406	0.9203	0.3709	0.9169	0.8333	0.8411	0.4167	0.9029
0.4545	0.8486	0.4545	0.8440	0.4696	0.9119	0.4707	0.9145	0.5000	0.9081	1.0000	0.7163	0.5000	0.8869
0.5455	0.8334	0.5455	0.8336	0.5900	0.8979	0.5813	0.9051	0.6204	0.9076			0.5833	0.8848
0.6364	0.8301	0.6364	0.8272	0.7007	0.8961	0.6996	0.8951	0.7505	0.8959			0.6667	0.8752
0.7273	0.8218	0.7273	0.8173	0.8297	0.8949	0.8221	0.8951	0.8698	0.8936			0.7500	0.8635
0.8182	0.8205	0.8182	0.8117	0.9523	0.8938	0.9403	0.8863	0.9718	0.8744			0.8333	0.8389
0.9091	0.8164	0.9091	0.8033										
1.0000	0.8122	1.0000	0.8060										

Table 9 Non dimensional load–frequency curves of the references [9, 10, 13, 16]

Musial [16]						Maeck et al. [10]				Van den Abeele and De Visscher [9]		Koh et al. [13]	
B-I		B-II		B-III		1		2		1		1	
λ	k_D	λ	k_D	λ	k_D	λ	k_D	λ	k_D	λ	k_D	λ	k_D
0.0008	1.0031	0.0008	1.0023	0.0013	1.0008	0.0000	1.0000	0.0000	1.0000	0.0000	1.0000	0.0000	1.0000
0.2807	0.9492	0.1404	0.9806	0.1880	0.9640	0.1379	0.9633	0.1581	0.9120	0.3333	0.9747	0.1099	1.0000
0.4185	0.8928	0.2552	0.9397	0.2475	0.9593	0.2586	0.8505	0.2372	0.8874	0.4333	0.9618	0.1099	0.9833
0.5556	0.8649	0.4211	0.8702	0.4156	0.8702	0.4138	0.7816	0.4743	0.8747	0.5000	0.9220	0.1542	0.8489
0.6963	0.8497	0.5631	0.8456	0.5547	0.8451	0.5517	0.7534	0.7115	0.8537	0.6667	0.9000	0.1713	0.8133
0.8379	0.8438	0.7030	0.8321	0.6930	0.8343	0.9655	0.7363	0.9486	0.8204	1.0000	0.8367	0.2055	0.7799
1.0000	0.7917	0.8446	0.8256	0.8317	0.8310			1.0000	0.7329			0.3088	0.7465
		1.0013	0.7894	1.0000	0.7714							0.6178	0.7111
												0.9979	0.7121

References

1. Wikipedia, List of bridge failures. https://en.wikipedia.org/wiki/List_of_bridge_failures. Accessed May 2014
2. Dimarogonas AD (1996) Vibration of cracked structures: a state of the art review. Eng Fract Mech 55(5):831–857. [https://doi.org/10.1016/S0141-0296\(96\)00175-8](https://doi.org/10.1016/S0141-0296(96)00175-8)
3. Salawu OS (1997) Detection of structural damage through changes in frequency: a review. Eng Struct 19(9):718–723. [https://doi.org/10.1016/S0141-0296\(96\)00149-6](https://doi.org/10.1016/S0141-0296(96)00149-6)
4. Doebling SW, Farrar CR, Prime MB, Shewitz DW (1996) Damage identification and health monitoring of structural

and mechanical systems from changes in their vibration characteristics: a literature review. LA-13070-MS, UC 900. Los Alamos National Laboratories, New Mexico

5. Yao YY, Shue-Ting TE, Glisic B (2014) Crack detection and characterization techniques—an overview. Struct Control Health Monit 21(12):1387–1413. <https://doi.org/10.1002/stc.1655>
6. Magalhães F, Cunha A, Caetano E (2012) Vibration based structural health monitoring of an arch bridge: from automated OMA to damage detection. Mech Syst Signal Process 28:212–228. <https://doi.org/10.1016/j.ymssp.2011.06.011>



7. Lianga Y, Lic D, Songd G, Fenga Q (2018) Frequency Co-integration-based damage detection for bridges under the influence of environmental temperature variation. *Measurement* 125:163–175. <https://doi.org/10.1016/j.measurement.2018.04.034>
8. Askegaard V, Langsø HE (1986) Correlation between changes in dynamic properties and remaining carrying capacity. *Mater Struct* 19(1):11–20
9. Van Den Abeele K, De Visscher J (2000) Damage assessment in reinforced concrete using spectral and temporal nonlinear vibration techniques. *Cem Concr Res* 30(9):1453–1464. [https://doi.org/10.1016/S0008-8846\(00\)00329-X](https://doi.org/10.1016/S0008-8846(00)00329-X)
10. Maeck J, Wahab MA, Peeters B, De Roeck G, De Visscher J, De Wilde WP, Ndambi J-M, Vantomme J (2000) Damage identification in reinforced concrete structures by dynamic stiffness determination. *Eng Struct* 22(10):1339–1349. [https://doi.org/10.1016/S0141-0296\(99\)00074-7](https://doi.org/10.1016/S0141-0296(99)00074-7)
11. Neild SA, Williams MS, McFadden PD (2003) Nonlinear vibration characteristics of damaged concrete beams. *ASCE J Struct Eng* 129(2):260–268. [https://doi.org/10.1061/\(ASCE\)0733-9445\(2003\)129:2\(260\)](https://doi.org/10.1061/(ASCE)0733-9445(2003)129:2(260))
12. Tan CM (2003) Nonlinear vibrations of cracked reinforced concrete beams. Ph.D. thesis, University of Nottingham. <http://eprints.nottingham.ac.uk/28976/1/275236.pdf>
13. Koh SJA, Maalej M, Quek ST (2004) Damage quantification of flexurally loaded RC slab using frequency response data. *Struct Health Monit* 3(4):293–311. <https://doi.org/10.1177/147592170400300401>
14. Massenzio M, Jacquelin E, Ovigne PA (2005) Natural frequency evaluation of a cracked RC beam with or without composite strengthening for a damage assessment. *Mater Struct* 38(10):865–873. <https://doi.org/10.1007/BF02482253>
15. Baghiee N, Esfahani MR, Moslem K (2009) Studies on damage and FRP strengthening of reinforced concrete beams by vibration monitoring. *Eng Struct* 31(4):875–893. <https://doi.org/10.1016/j.engstruct.2008.12.009>
16. Musiał M (2012) Static and dynamic stiffness of reinforced concrete beams. *Arch Civ Mech Eng* 12(2):186–191. <https://doi.org/10.1016/j.acme.2012.04.005>
17. Hamad WI, Owen JS, Hussein MFM (2014) Modelling the degradation of vibration characteristics of reinforced concrete beams due to flexural damage. *Struct Control Health Monit* 22(6):939–967. <https://doi.org/10.1002/stc.1726>
18. Belluzzi O (1960) *Scienza delle Costruzioni*, vol I–IV. Zanichelli, Bologna. ISBN 978-8-808-01256-2
19. Benedetti A, Nichols JM, Tomor A (2016) Influence of environmental degradation on dynamic properties of masonry bridges. In: 16th IB2MAC conference, Padua, Italy
20. Newton M, Johnson GP, Enomoto BT (2006) Fundamental frequency testing of reinforced concrete beams. *J Perform Constr Facil* 20(2):196–200. [https://doi.org/10.1061/\(ASCE\)0887-3828\(2006\)20:2\(196\)](https://doi.org/10.1061/(ASCE)0887-3828(2006)20:2(196))
21. Castel A, Gilbert RI, Ranzi G (2014) Instantaneous stiffness of cracked reinforced concrete including steel-concrete interface damage and long-term effects. *J Struct Eng* 140(6):1–9. [https://doi.org/10.1061/\(ASCE\)ST.1943-541X.0000954](https://doi.org/10.1061/(ASCE)ST.1943-541X.0000954)
22. Xu T, Castel A (2016) Modeling the dynamic stiffness of cracked reinforced concrete beams under low-amplitude vibration loads. *J Sound Vib* 368:135–147. <https://doi.org/10.1016/j.jsv.2016.01.007>
23. Chondros TG, Dimarogonas AD, Yao J (2001) vibration of a beam with a breathing crack. *J Sound Vib* 239(1):57–67. <https://doi.org/10.1006/jsvi.2000.3156>
24. Bendat JS (1998) *Nonlinear systems techniques and applications*. Wiley, New York. ISBN 978-0-471-16576-7
25. Bayissa WL, Haritos N (2005) Experimental investigation into vibration characteristics of a cracked RC T-beam. In: 4th Australasian congress on applied mechanics, Melbourne, Australia, pp 263–269
26. Kim H, Melhem H (2003) Fourier and wavelet analyses for fatigue assessment of concrete beams. *Exp Mech* 43(2):131–140. <https://doi.org/10.1007/BF02410494>
27. Gao Y, Du Y, Jiang Y, Zhao W (2017) Research on cracking of reinforced concrete beam and its influence on natural frequency by expanded distinct element method. *J Aerosp Eng* 30(2):B4016015–B4016017. [https://doi.org/10.1061/\(ASCE\)AS.1943-5525.0000703](https://doi.org/10.1061/(ASCE)AS.1943-5525.0000703)